Journal of Physics: Conference Series **75** (2007) 012023 doi:10.1088/1742-6596/75/1/012023

Simulating Dynamic Stall in a 2D VAWT: Modeling strategy, verification and validation with Particle Image Velocimetry data

C.J. Simão Ferreira, H. Bijl, G. van Bussel, G. van Kuik

DUWIND- Delft University Wind Energy Research Institute, Kluyverweg 1, 2629 HS Delft, NL

E-mail: c.j.simaoferreira@tudelft.nl

Abstract.

The implementation of wind energy conversion systems in the built environment renewed the interest and the research on Vertical Axis Wind Turbines (VAWT), which in this application present several advantages over Horizontal Axis Wind Turbines (HAWT). The VAWT has an inherent unsteady aerodynamic behavior due to the variation of angle of attack with the angle of rotation, perceived velocity and consequentially Reynolds number. The phenomenon of dynamic stall is then an intrinsic effect of the operation of a Vertical Axis Wind Turbine at low tip speed ratios, having a significant impact in both loads and power.

The complexity of the unsteady aerodynamics of the VAWT makes it extremely attractive to be analyzed using Computational Fluid Dynamics (CFD) models, where an approximation of the continuity and momentum equations of the Navier-Stokes equations set is solved.

The complexity of the problem and the need for new design approaches for VAWT for the built environment has driven the authors of this work to focus the research of CFD modeling of VAWT on:

- comparing the results between commonly used turbulence models: *URANS* (*Spalart-Allmaras* and k-ϵ) and *large eddy* models (*Large Eddy Simulation* and *Detached Eddy Simulation*)
- verifying the sensitivity of the model to its grid refinement (space and time),
- evaluating the suitability of using Particle Image Velocimetry (PIV) experimental data for model validation.

The 2D model created represents the middle section of a single bladed VAWT with infinite aspect ratio. The model simulates the experimental work of flow field measurement using Particle Image Velocimetry by Simão Ferreira et al [1] for a single bladed VAWT.

The results show the suitability of the PIV data for the validation of the model, the need for accurate simulation of the large eddies and the sensitivity of the model to grid refinement.

Nomenclature

c	airfoil/blade chord, [m]
C_N	normal force, [-]
C_T	tangential force, [-]
D	rotor diameter, [m]
k	reduced frequency, [-]
R	rotor radius, [m]

Re	Reynolds number, [-]
U_∞	Unperturbed velocity, [m/s]
DES	Detached Eddy Simulation
LES	Large Eddy Simulation
RANS	Reynolds-Averaged Navier-Stokes
URANS	Unsteady Reynolds-Averaged Navier-Stokes)
α	angle of attack, [°]
θ	azimuth angle, [°]
ω	angular velocity of the rotor frequency, [rad/s]
Ω	vorticity, $[s^{-1}]$
Γ	circulation, $[m^2/s]$
ρ	density of the fluid, $[kg/m^3]$
μ_Γ	average value of circulation, $[m^2/s]$

1. Introduction

The increasing awareness of the need for environmentally sustainable housing and cities has driven the promotion of wind energy conversion systems for the built environment. One of the results of the development of solutions for the built environment is the reappearance of Vertical Axis Wind Turbines (VAWTs). In the built environment, the VAWT presents several advantages over the more common Horizontal Axis Wind Turbines (HAWTs), namely: its low sound emission (consequence of its operation at lower tip speed ratios), better esthetics due to its three-dimensionality, its insensitivity to yaw wind direction and its increased power output in skewed flow (see Mertens et al [2] and Simão Ferreira et al [3]).

The phenomenon of dynamic stall is an inherent effect of the operation of a VAWT at low tip speed ratios (λ). The presence of dynamic stall has significant impact on both load and power.

Modeling the VAWT in dynamic stall presents five immediate challenges:

- The unsteady component of the flow requires a time accurate model, adding an extra dimension (time) to the numerical grid.
- The geometry of the rotor does not allow for important spatial/time grid simplifications to be applied (example: moving reference frames or radial symmetry).
- The large amount of shed vorticity implies that the model could be sensitive to numerical dissipation.
- The geometry of a Vertical Axis Wind Turbine results in blade-vortex interaction at the downwind passage of the blade between the blade and the shed vorticity that was generated at the upwind passage. This means that the development of the shed vorticity must be correctly modeled inside the entire rotor diameter; in order to avoid numerical dissipation, the spatial resolution of the grid must be very fine not only in the immediate vicinity of the blades but over the entire rotor.
- The variation of angle of attack of the blade with azimuth angle implies a varying relation/dominance between lift and drag force on the blade (resulting in instants during the rotation where the VAWT is actually being decelerated because only drag force is present). The correct use of a turbulence model and near-wall models is essential in these situations. This is particulary important at low tip speed ratios, where the power output of the VAWT is negative (for a certain range of λ); the performance at low tip speed ratios is highly important for start-up behavior, one of the disadvantages usually associated with VAWT.

This numerical model aims at simulating the experimental work by Simão Ferreira et al [1],for conditions of $Re = 50000$ and tip speed ratio $\lambda = 2$, continuing the work presented in [4].

Contrary to the previous attempts to model the VAWT using CFD (see Hansen et al [5] , Allet et al [6] , Paraschivoiu et al [7] , Paraschivoiu et al [8] and Paraschivoiu [9]), the validation of the results is achieved not by comparing the load on the blades but by comparing the vorticity in the rotor area. This work aims also at demonstrating the suitability of PIV data for validation of numerical models for this specific problem.

The results of the simulations show the impact of choice of turbulence model and grid refinement.

2. Model geometry and computational grid

The geometry of the model is a 2D representation of the experimental setup of Simão Ferreira et al [1]. The CFD grid presents a slight discrepancy later discovered between the location of the airfoil in relation to the radial direction used in the experiment; further calculations showed this discrepancy to be negligible in validation of the results and its implications. The model's wall boundary conditions consists of two walls spaced $1.25m$ apart, where a $0.4m$ diameter single-bladed Darrieus VAWT is placed. The rotor is represented by an $0.05m$ chord $NACA0015$ airfoil and the $0.05m$ rotor axis. The rotor axis is placed over the symmetry position of the wind tunnel. The inlet and outlet boundary conditions are placed respectively $10D$ upwind and $14D$ downwind of the rotor, allowing a full development of the wake.

The model comprises a 2D spatial grid, simulating the conditions at the middle cross-section of the experimental setup. The grid is composed of four non-conformal sub-grids, each a structured grid of quadrilateral elements. Figure 1 presents a diagram of the shape and location of each sub-grid and the wall boundary conditions representing the airfoil/blade, wind tunnel walls and rotor axis (the flow inlet and outlet boundary conditions are not represented).

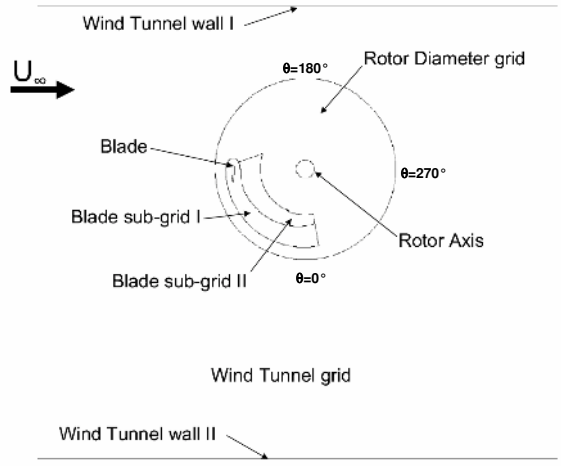

Figure 1. Diagram of the model geometry, sub-grid distribution and boundary conditions.

The use of moving sub-grids is necessary due to the movement of the rotor elements. Thus, the sub-grids *Rotor Diameter*, *Blade sub-grid I*, and *Blade sub-grid II* rotate with an angular velocity $\omega = 75rad/s$, while the sub-grid *Wind Tunnel* remains fixed. The option of dividing the rotor space in three non-conformal sub-grids allows the use of a structured grid without compromising its quality or requiring a large mesh with over refinement in areas of lower importance. A quadrilateral structured grid also allows easier control of the refinement of the grid; this aspect is crucial in the present work, since the sensitivity to the refinement of the space grid is evaluated.

The most refined sub-grid is *Blade sub-grid I* which defines the geometry of the airfoil and its immediate wake development flow region. The reference fine grid comprises 3305 nodes over the airfoil surface, where the height of the first row of cells is set at a distance to the wall of

$0.02\%c$ to ($y^+ \approx 1$ when $\theta = 90°$, $k-\epsilon$ model). The total model size comprises approx. $1.6 * 10^6$ cells.

3. Simulated flow conditions

The simulation aimed at representing the flow conditions of the experimental work for $\lambda = 2$ and incoming flow $U_\infty = 7.5m/s$. The level of unsteadiness is determined by the reduced frequency k, defined as $k = \omega.c/2V$, where ω is the angular frequency of the unsteadiness, c is the blade's chord and V is the velocity of the blade. In this experiment, due to the variation of V with rotation angle, k was defined as $k = \omega.c/(2.\lambda.V_\infty) = \omega.c/(2.\omega.R) = c/(2.R)$, where λ is the tip speed ratio and R is the radius of rotation. For this experimental work $k = 0.125$, placing the work in the unsteady aerodynamics region.

Due to the importance of the induction of the rotor, it is necessary to perform a simulation for several rotations until a fully developed wake is present. All values presented in this paper relate to the revolutions of the rotor after a periodic post-transient solution is found.

4. Validation of the results of different turbulence models

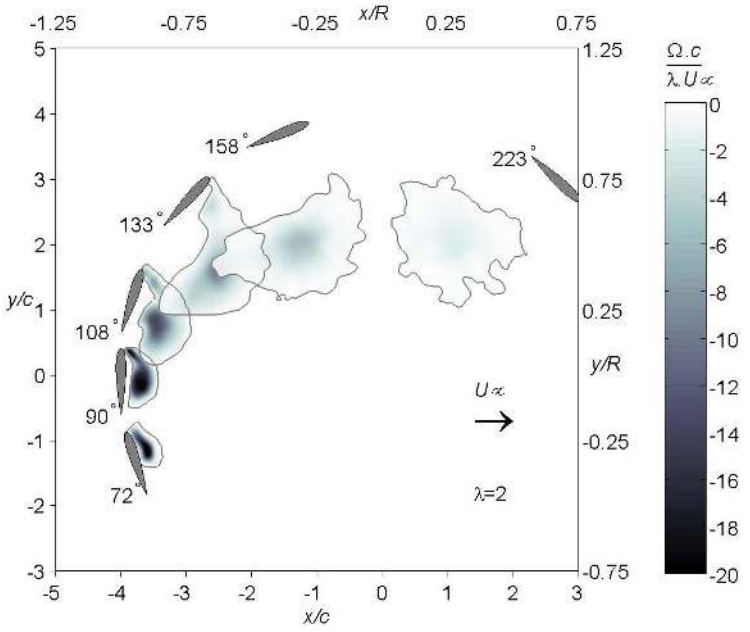

Figure 2. PIV experimental data of the evolution of the circulation of leading edge separated vortex for $\lambda = 2$ at 90°, 108°, 133° and 158°).

Four different turbulence models where used in this work, complementing the analysis with a *Laminar* model by Simão Ferreira et al [4]; two *URANS* (Spallart-Almaras and k-ϵ) and two *large eddy* models (*DES* and *LES*).

The simulations results are validated against the experimental results of Simão Ferreira et al [1] for the case of $\lambda = 2$. These results, of which Figures 2 and 3 are an example, show that the flow is characterized by the shedding to the flow of strong vortices; this shedding of vorticity is located:

- at the leading edge, resulting of a leading edge separation where the clockwise vortices detach from the surface
- at the trailing edge, where a wake is formed from the pressure side boundary layer and the boundary layer developed in the suction side after the point of leading edge separation-reattachment; this wake experiences a roll up due to the strong vorticity.

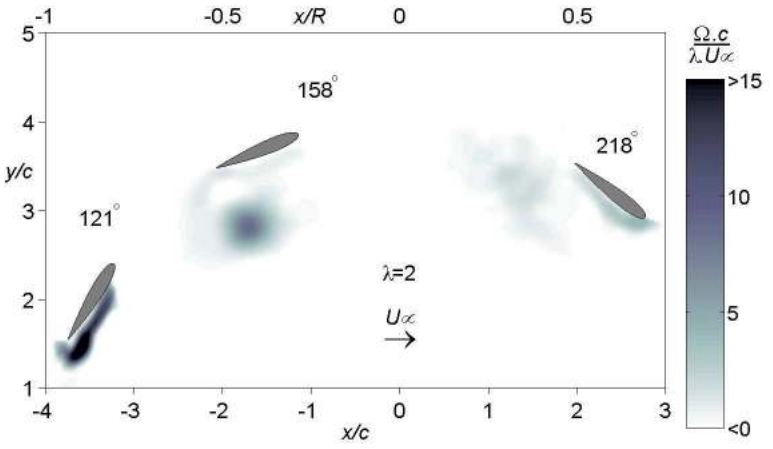

Figure 3. PIV experimental data of the evolution of the counter-clockwise vorticity shed after the roll-up of the trailing edge vorticity.

The validation of the simulations compares the vorticity field in the vicinity of the airfoil at two azimuthal angles: $\theta = 90^\circ$ and $\theta = 120^\circ$; the choice of these two moments of the rotation is driven by the development of the vorticity shed from the leading edge and the wake at the trailing edge. Taking into account the experimental results, the two azimuthal positions define:

- at $\theta = 90^\circ$ the vorticity shed at the leading edge has rolled in a large conglomerate of small vortices in an region one chord length; yet, the wake at the trailing edge has not yet started to roll up nor moving over the suction surface
- at $\theta = 120^\circ$ the wake shed at the trailing edge has rolled up and the main counter-clockwise vorticity is over the last quarter of the suction side of the airfoil, between the surface and the leading edge shed vorticity which as started to be convected away from the airfoil.

4.1. URANS models

Unsteady Reynolds-Averaged Navier-Stokes aims at reducing the computational effort by solving the Reynolds averaged form of the Navier-Stokes equations (see Bredberg [10]), however requiring the modeling of the Reynolds stresses originated from the averaging method. In the range of possible models are *eddy-viscosity models* which assume that the Reynolds stresses can be estimated by a relation of the *eddy viscosity* ν_t and the velocity spatial derivatives. In this work two of the most popular *URANS eddy viscosity* models are used: the one-equation *Spallart-Almaras* (*S-A*) and the two-equations k-ϵ model. The *S-A* used is the implementation in the CFD package Fluent (see reference [11]) of the model proposed by Sparllat and Almaras [12]. The k-ϵ model is the standard implementation in Fluent [11] referred as *Standard* k-ϵ.

Previous attempts on the simulation of $2D$ VAWT flow (see Hansen et al [5] , Allet et al [6] , Paraschivoiu et al [7] , Paraschivoiu et al [8] and Paraschivoiu [9])) have resorted to these or similar models; the results presented in this paper using *URANS* are thus a link between previous research and the application of more complex models such as *LES* and *DES*.

Figures 4 and 5 show the vorticity field in the vicinity of the airfoil at $\theta = 90^\circ$ and $\theta = 120^\circ$. Comparing with the experimental results, the *S-A* model underestimates the generation and shedding of vorticity at the leading edge (in the simulation the leading edge shed vorticity is only located in the first half of the airfoil while experimental results show it covering the entire airfoil length - Figure 2); it is also unable to predict the roll-up of the trailing edge shed vorticity clearly seen in the experimental work (Figure 3) even at $\theta = 120^\circ$. The k-ϵ model (Figures 6 and 7), although more computationally expensive, is also not able to predict these two main phenomena of the flow field. The option of both models of simulating all scales of turbulence based on the Boussinesq hypothesis of isotropy of the turbulence clearly proved to be

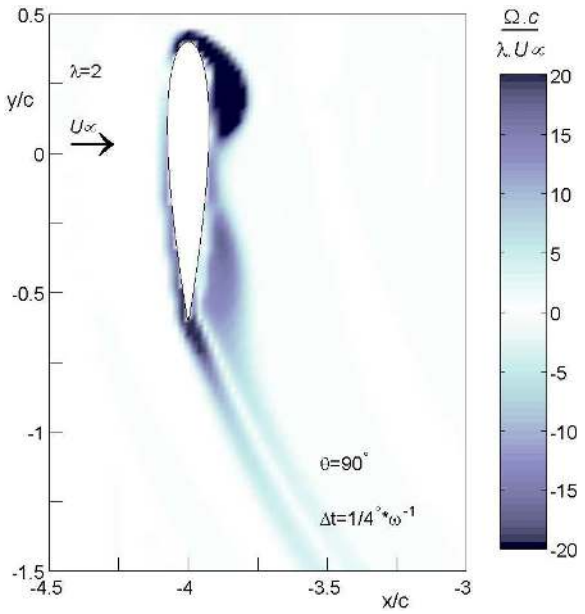

Figure 4. Vorticity field at $\theta = 90°$, *Spalart-Allmaras* model.

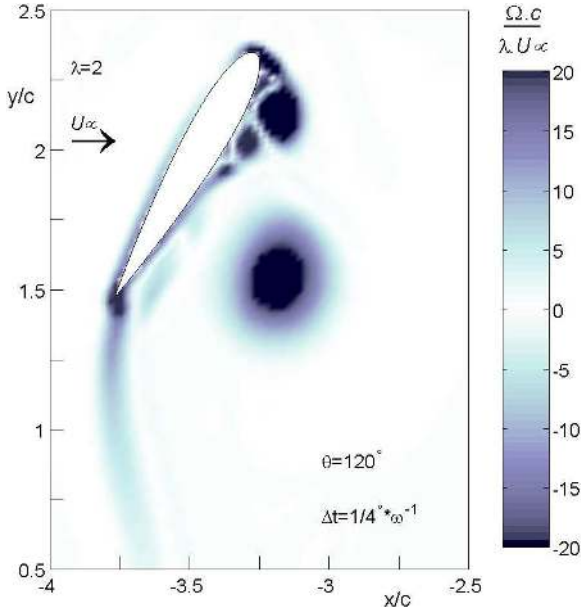

Figure 5. Vorticity field at $\theta = 120°$, *Spalart-Allmaras* model.

insufficient for the dominant large scales of the flow field. The verification of time grid refinement (with the *S-A* model) lead to two observations: the refinement did not produce any significant improvement in the prediction of the vorticity shed phenomena; and a time step of $\Delta t = 1/4°/\omega$ is recommended as maximum time step for a relevant simulation.

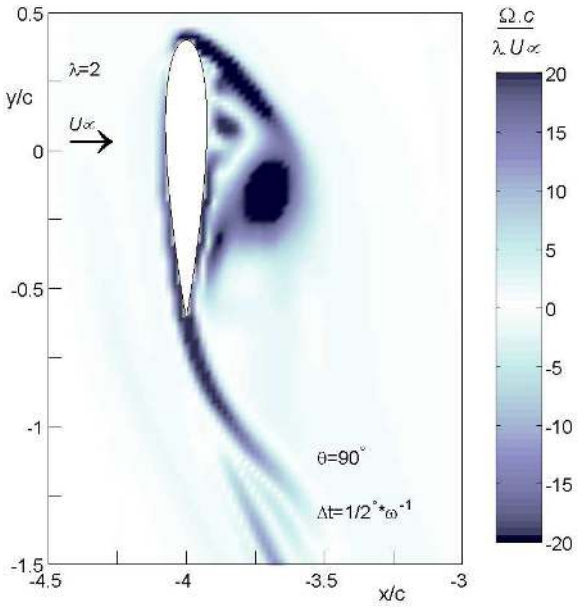

Figure 6. Vorticity field at $\theta = 90°$, $k - \epsilon$ model.

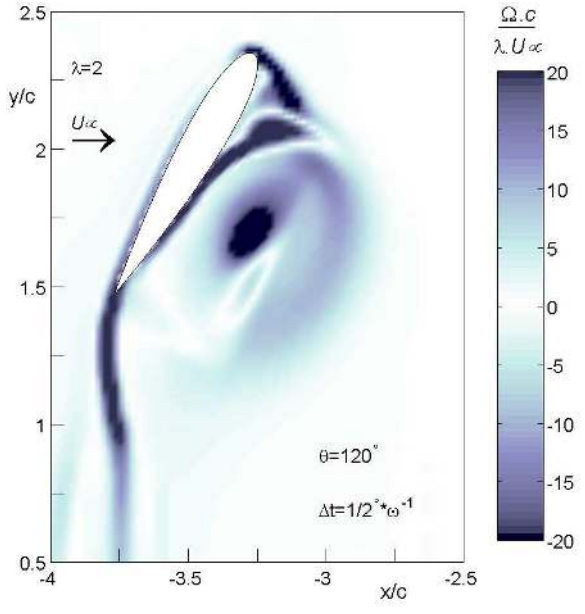

Figure 7. Vorticity field at $\theta = 120°$, $k - \epsilon$ model.

4.2. LES

The *Large Eddy Simulations* used is the standard model implemented in Fluent [11] for $2D/3D$ simulation. Contrary to *URANS*, in *LES* the equations are not Reynolds-averaged in time, but are space filtered (averaged in volume). This operation implies an increase of the computational requirements, but reduces the turbulence modeling to only the sub-grid scale (*SGS model*), solving the larger scales of turbulence. The *SGS* model used is the Smagorinsky-Lilly model [11], which is a one equation eddy-viscosity model. One of current limitations of *LES* is its wall treatment, where the *SGS* model is commonly applied (see Spalart [13]). The required refinement of the grid at the wall for a correct simulation of all the scales using *LES* is still too computationally expensive (although one might argue that for a 2D model at moderate Reynolds some cases are feasible). Attempts to model unsteady airfoil flows with *LES* (Dahlström et al [14]) have shown the feasibility of using LES but raised some challenges regarding the choice of *SGS* models and artificial unsteadiness.

Figures 8 and 9 show the vorticity distribution around the airfoil for $\theta = 90°$ and $\theta = 120°$. In this simulation, the large shedding of leading edge vorticity and the roll-up of the trailing edge wake are simulated (a clear improvement over the *URANS* model); yet, the location of the vorticity shed at the leading edge covers a larger area than what was observed in the experimental results and the roll-up of the trailing edge wake occurs too early in the rotation; in the experiments the roll-up of the trailing edge wake starts at $\theta = 120°$ (Figure 3), while in the simulation it can already be seen at $\theta = 90°$ (Figure 8).

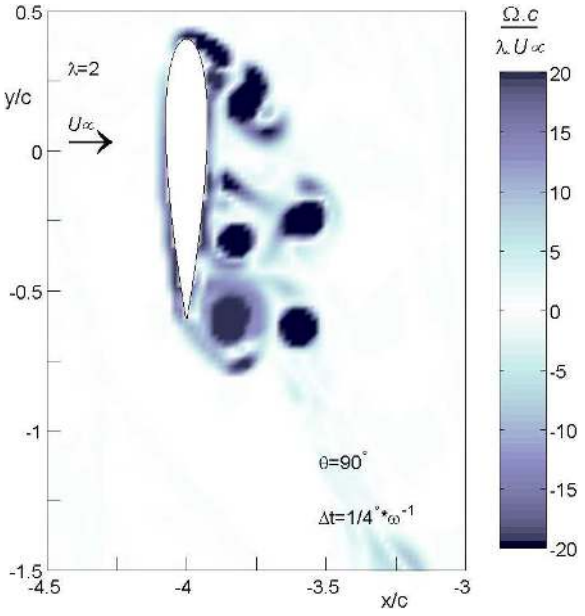

Figure 8. Vorticity field at $\theta = 90°$, *Large Eddy Simulation*

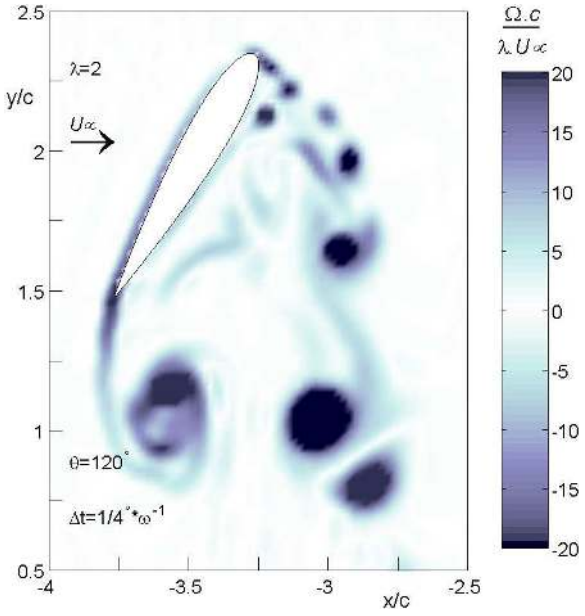

Figure 9. Vorticity field at $\theta = 120°$, *Large Eddy Simulation*

4.3. DES

Detached-Eddy Simulations used is, as implemented in Fluent in $2D/3D$ formulation, a hybrid method of *LES* and *URANS*, where the wall region is modeled with a *URANS* model and the outer region with *LES*; the motivation for using *DES* is the high cost of *LES* in the boundary layer region. In the present work, an *S-A* model is used for the wall region‘[11].

Figures 10 and 11 show the vorticity distribution around the airfoil for $\theta = 90°$ and $\theta = 120°$. Of all the models used, the *DES* simulations present the results best agreeing with experiments;

the region and location of the turbulence and the phase of roll up of the trailing edge wake are as experimentally observed.

The reason for the improvement in relation to the *LES* can only be accounted by a more correct modelling of the wall region, even when using a single equation *S-A* model, implying that the $y^+ \approx 1$ scale is still too course for an *LES* simulation. Yet, the influence of grid refinement in *DES* and what it implies in the validity of the model can pose a challenge (see Spalart [15]). Results of verification of grid sensitivity shall be presented further on this paper.

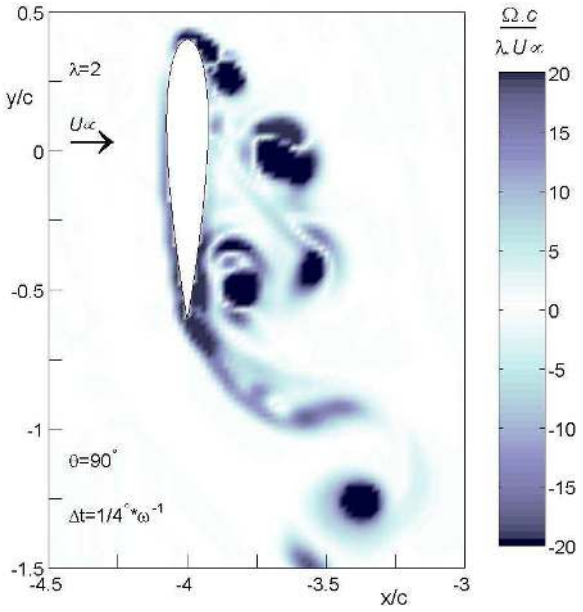

Figure 10. Vorticity field at $\theta = 90°$, *Detached Eddy Simulation.*

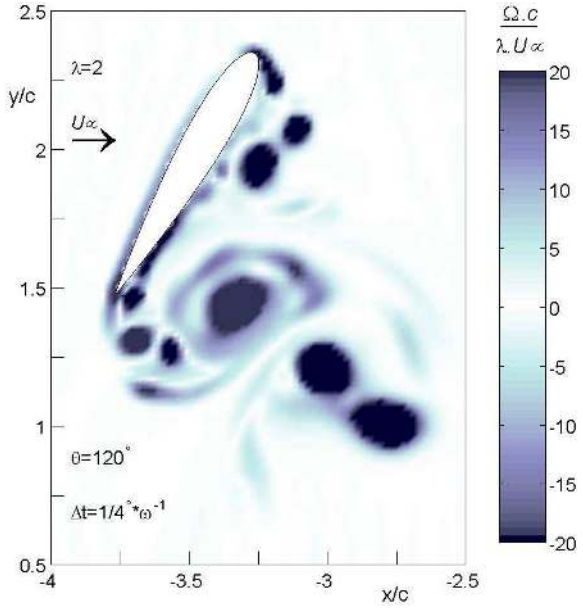

Figure 11. Vorticity field at $\theta = 120°$, *Detached Eddy Simulation.*

5. Comparison of force simulation

The models have until now been analyzed by comparing the evolution of the shed vorticity with experimental observations. The values of tangential and normal force [1] will now be compared in Figures 12,13,14 and 15. Three main differences are visible between the *URANS* models and the large eddy models *DES* and *LES*:

- a non-zero value of normal force at $\theta = 0$ for both *URANS* models, thus representing a large value of lift at a zero geometric angle of attack; in both the *DES* and *LES* models the value of the force is zero
- the azimuthal location of the maxima of tangential and normal forces: in the *DES* and *LES* models both tangential and normal forces reach a maximum at lower values of θ (in compared with the *URANS* models), followed by an almost linear decrease with θ; the failure of the *URANS* models to capture this effect might lay on their inability to correctly model the development of vorticity around the airfoil
- the level of unsteadiness of the forces; the *DES* and *LES* present large oscillations in the forces at frequencies higher than the frequency of rotation of the turbine; this might be a result of the shedding of strong small vortices in the *DES* and *LES* as opposed to a single

[1] Tangential force is considered in the direction of rotation of the blade and normal force in the radial direction.

continuous vortex in the *URANS* models; yet, numerical convergence effects can also be in the origin of these fluctuations.

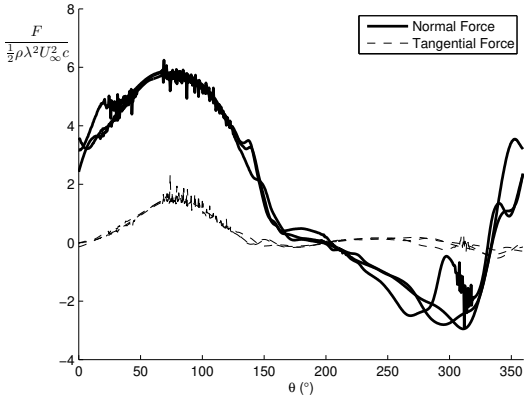

Figure 12. Tangential and Normal force in the blade, SA model, $\Delta t = 1/2^\circ/\omega$. Instantaneous values over three rotations.

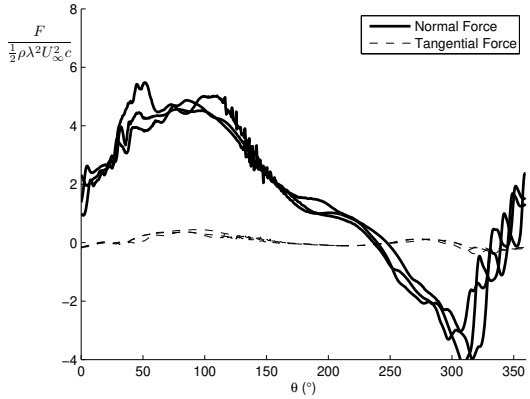

Figure 13. Tangential and Normal force in the blade, $k-\epsilon$ model, $\Delta t = 1/2^\circ/\omega$. Instantaneous values over three rotations.

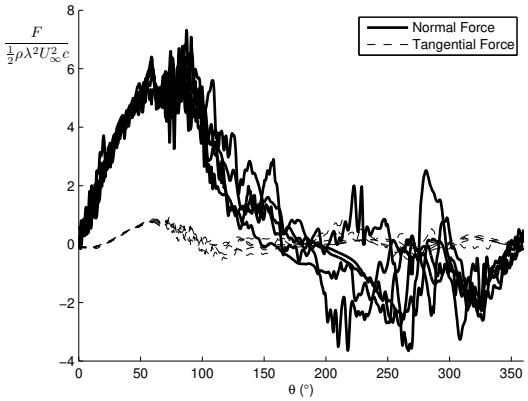

Figure 14. Tangential and Normal force in the blade, DES, $\Delta t = 1/4^\circ/\omega$. Instantaneous values over five rotations.

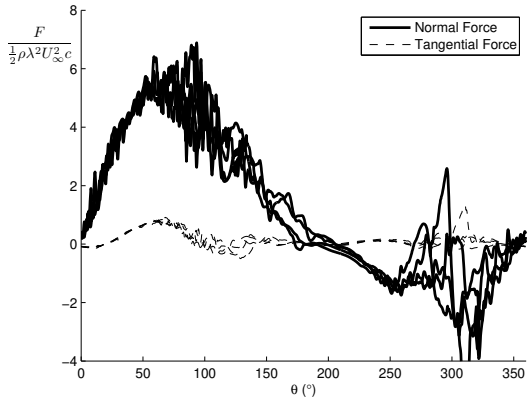

Figure 15. Tangential and Normal force in the blade, LES model, $\Delta t = 1/4^\circ/\omega$. Instantaneous values over four rotations.

6. Verification to grid sensitivity

The work of Simão Ferreira et al [4] presented an evaluation of the effect of space and time grid refinement/coarsening for the case of a *Laminar* model; such evaluation showed a high sensitivity of the results to the refinement of the grid. Yet, the *DES* model has proved to be a more suitable simulation tool; thus, in this section, we shall evaluate the robustness of the *DES* simulation towards grid refinement.

6.1. Time grid refinement

In the reference simulation, a time step $\Delta t = 1/4^\circ\omega^{-1}$ is used. The analysis now presented compares this simulation with two other with the same initial conditions but time steps

$\Delta t = 1/8°\omega^{-1}$ and $\Delta t = 1/16°\omega^{-1}$.

Figures 16 and 17 present the vorticity distribution at $\theta = 90°$. Similarly to what it was observed by Simão Ferreira et al [4] with a *Laminar* model, also for the *DES* model the first refinement of the time step ($\Delta t = 1/8°\omega^{-1}$) results in a overgeneration of the vorticity and an early roll-up of the wake at the trailing edge; yet, the second refinement ($\Delta t = 1/16°\omega^{-1}$) does not consecutively generate another increase; in fact the differences between the two results are minimal and in what is expected in relation to the randomness of the flow. This interpretation of the results is also confirmed by the simulated force values (Figure 18). The *DES* simulation appears to be less sensitive to time grid refinement at this magnitude of step size.

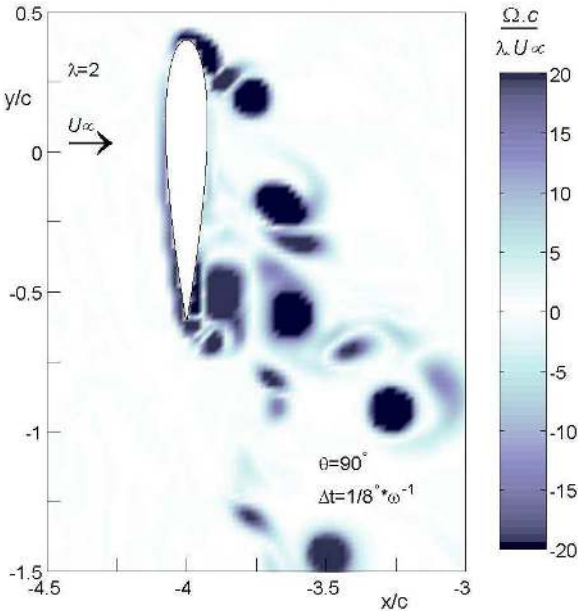

Figure 16. Vorticity field at $\theta = 90°$, $\Delta t = 1/8°\omega^{-1}$.

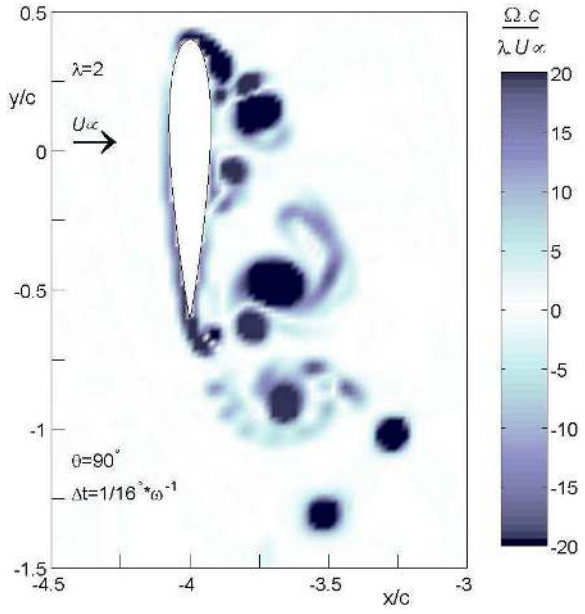

Figure 17. Vorticity field at $\theta = 90°$, $\Delta t = 1/16°\omega^{-1}$.

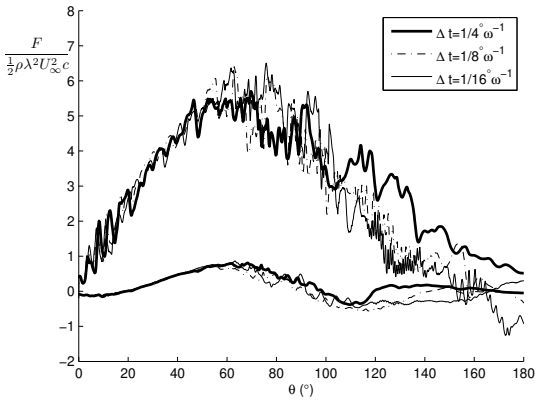

Figure 18. Effect on tangential and normal force of change of the time grid refinement.

6.2. Space grid refinement

In the work of Simão Ferreira et al [4], the space grid coarsening applied on the *Laminar* model resulted in an over generation of vorticity and an earlier roll-up of the trailing edge wake at

$\theta = 90°$. In the current work using a *DES* model, two simulations where performed with coarser space meshes (x and y); only *Blade sub-grid I* was coarsened, in the first case by quadrupling the cell area ($4\Delta A$, doubling height and width) and in the second case by sixteenfold ($16\Delta A$, quadrupling height and width).

The results showed in Figures 19, 20 and 21 shows that the overgeneration of vorticity and is also present when using a *DES* model; however, the variation is not as large as observed in the laminar model and the effect on the force is small.

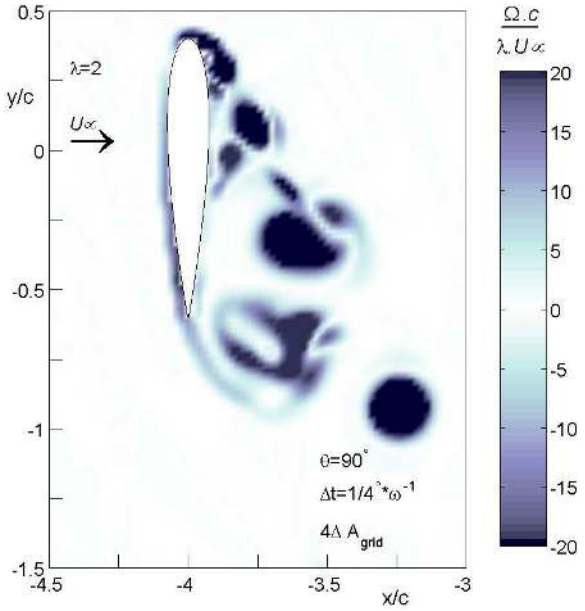

Figure 19. Vorticity field at $\theta = 90°$, $\Delta t = 0.25°/\omega$, 2 times coarser grid.

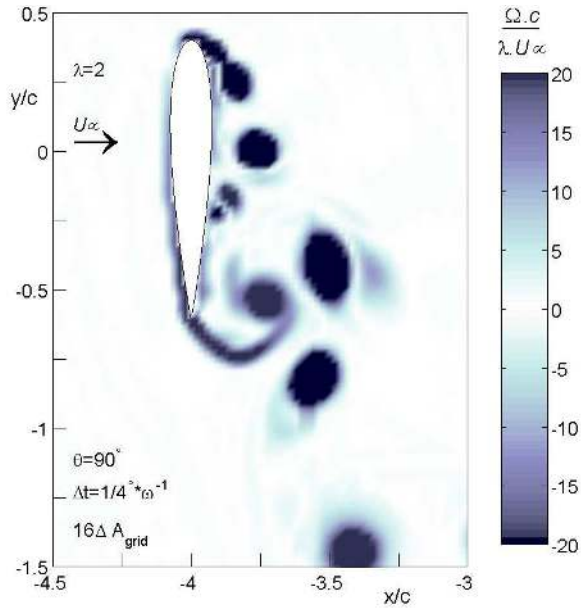

Figure 20. Vorticity field at $\theta = 90°$, $\Delta t = 0.25°/\omega$.

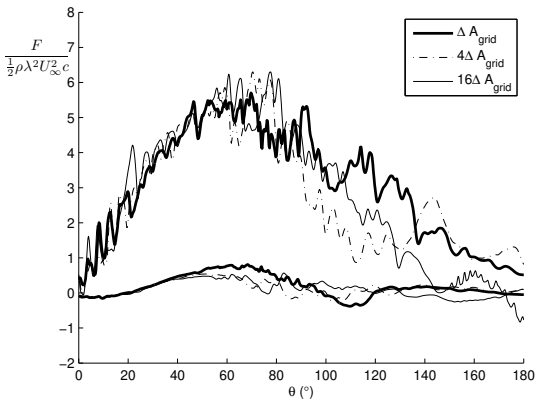

Figure 21. Effect on tangential and normal force of change of the space grid refinement.

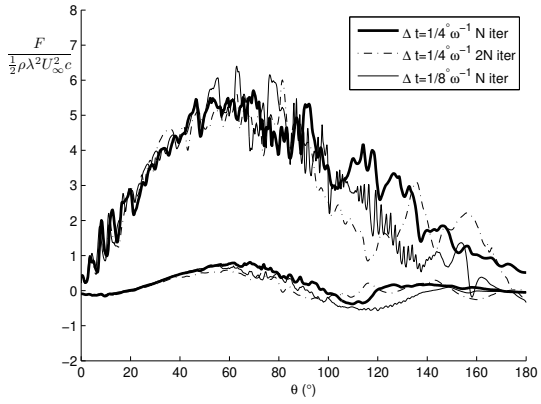

Figure 22. The effect of convergence on tangential and normal force of change of the convergence iteration.

7. Verification convergence error

The oscillations observed in the force output at frequencies much higher than the rotational frequency can have two origins:

- a real physical behavior resulting from the continuous shedding of strong small vortices over the surface and at the trailing edge
- a numerical convergence problem, where for each time step, the solution converges slightly faster or slower, thus undershooting or overshooting the real value.

To observe the validity of the later, three simulations of a half rotation starting at the same initial condition are compared (Figure 22). The three solutions encompass:

- the reference model, with $\Delta t = 1/4^{\circ}\omega^{-1}$ and N iterations per time step
- a second model, with $\Delta t = 1/4^{\circ}\omega^{-1}$ and $2N$ iterations per time step
- a time refined model, with $\Delta t = 1/8^{\circ}\omega^{-1}$ and N iterations per time step.

The results do not present any large change on the amount of high frequency oscillations on the force curve, with the main difference between the curves occurring past the roll up of the trailing edge vorticity at $\theta > 90^{\circ}$. The comparison does not allow us to draw any conclusion regarding the effect of convergence, and more research is required.

8. Conclusions

The results demonstrate the influence of different turbulence models on the accuracy of the prediction of dynamic stall development on a VAWT. Of the models analyzed, the *Detached Eddy Simulation* turbulence model presented the results closest to experiments. The *DES* model is not only able to predict the generation and shedding of vorticity and it's convection, it also shows an acceptable sensitivity to grid refinement (both space and time), thus making it suitable for simulations where validation data is limited or non existent. *URANS* models proved insufficient due to their inability of correctly modeling the large eddies. The *LES* performed worse than than the *DES* model, probably due to a less accurate modeling of the wall region.

The high frequency (in comparison to the rotational frequency) oscillations of the forces on the airfoil might indicate a numerical oscillation of the convergence of the solution in each time step. Simulations aimed at testing this hypothesis did not reach any final conclusion, since the differences between the various grid refinements are in the range of randomness of the simulation, but prove the need for a experimental study of the time development of forces and possible frequency analysis.

The numerical work proves the usefulness of velocity data (in this case acquired with PIV) for validation. The visualization of the shedding and convection of the vorticity (in particular the location of the leading edge vorticity and the moment of roll up of the trailing edge vorticity) prove to be more specific for validation than the comparison of the force on the blade; in simulations with varying grid refinement, the simulations presented different behaviors of the flow field, clearly identifiable in comparison with experimental data. Yet, the result of the integral forces on the airfoil did not present differences outside the uncertainty range associated with the randomness of the flow.

Future research will focus on developing modeling guidelines applying *DES*, focusing on:

- limiting the uncertainty associated with grid refinement,
- testing the different turbulence sub-models and wall treatment models,
- applying simulation for performance evaluation of different airfoil shapes (camber and thickness effects),
- analyze the influence of wall models, with special focus on the calculation of friction drag.

9. Acknowledgments
The authors would like to thank Dr. van Zuijlen (DUWIND) for his insightful help and remarks.

10. Bibliography
[1] C.J. Simão Ferreira, G. van Bussel, and G. van Kuik. 2D PIV visualization of dynamic stall on a vertical axis wind turbine. In 45^{th} *AIAA Aerospace Sciences Meeting and Exhibit /ASME Wind Energy Symposium*, 2007.
[2] S. Mertens, G. van Kuik, and G. van Bussel. Performance of a H-Darrieus in the skewed flow on a roof. *Journal of Solar Energy Engineering*, 125:433–440, 2003.
[3] C.J. Simão Ferreira, G. van Bussel, and G. van Kuik. Wind tunnel hotwire measurements, flow visualization and thrust measurement of a VAWT in skew. In 44^{th} *AIAA Aerospace Sciences Meeting and Exhibit /ASME Wind Energy Symposium*, 2006.
[4] C.J. Simão Ferreira, G. van Bussel, and G. van Kuik. 2D CFD simulation of dynamic stall on a Vertical Axis Wind Turbine: verification and validation with PIV measurements. In 45^{th} *AIAA Aerospace Sciences Meeting and Exhibit /ASME Wind Energy Symposium*, 2007.
[5] M.O.L. Hansen and D.N. Søresen. CFD model for Vertical Axis Wind Turbine. In *Wind Energy for the New Millennium-Proceedings of the European Wind Energy Conference, Copenhagen, Denmark*, 2001.
[6] A. Allet, S. Hallé, and I. Paraschivoiu. Numerical simulation of dynamic stall around an airfoil in Darrieus motion. *Journal of Solar Energy Engineering*, 121:69–76, February 1999.
[7] I. Paraschivoiu and A. Allet. Aerodynamic analysis of the Darrieus wind turbines including dynamic-stall effects. *Journal of Propulsion and Power*, 4(5):472–477, 1988.
[8] I. Paraschivoiu and C. Béguier. Visualization, measurements and calculations of dynamic stall for a similar motion of VAWT. In *Proceedings of the European Wind Energy Conference, Herning, Denmark*, 1998.
[9] I. Paraschivoiu. *Wind Turbine Design - With Emphasis on* D*arrieus Concept*. Polytechnic international Press, 2002.
[10] Jonas Bredberg. On two equation eddy-viscosity models. Technical Report 01/8, Chalmers University of Technology, Göteborg, Sweden, 2001.
[11] *Fluent User's Manual*. Fluent Inc.
[12] P. R. Spalart and S. Almaras. A one-equation turbulence model for aerodynamic flows. Technical Report AIAA-92-0439, American Institute of Aeronautics and Astronautics, 1992.
[13] P. R. Spalart. Strategies for turbulence modelling and simulations. *International Journal of Heat and Fluid Flow*, 21:252–263, 2000.
[14] S. Dahlström and L. Davidson. Large eddy simulation of the flow around an airfoil. In *39th* AIAA *Aerospace Sciences Meeting and Exhibit*, 2001.
[15] P. R. Spalart. Topics in detached-eddy simulation. In *Computational Fluid Dynamics 2004*. Springer Berlin Heidelberg, 2006.